Journal of Geodynamics 88 (2015) 14–22

Contents lists available at ScienceDirect

Journal of Geodynamics

journal homepage: http://www.elsevier.com/locate/jog

Applying local Green's functions to study the influence of the crustal structure on hydrological loading displacements

R. Dill[a,*], V. Klemann[a], Z. Martinec[b,c], M. Tesauro[a,d]

[a] Helmholtz Centre Potsdam – GFZ German Research Centre for Geosciences, Section 1.3: Earth System Modelling, Germany
[b] Charles University in Prague, Czech Republic
[c] DIAS – Dublin Institute of Advanced Studies, Ireland
[d] Utrecht University, The Netherlands

ARTICLE INFO

Article history:
Received 10 December 2014
Received in revised form 9 March 2015
Accepted 8 April 2015
Available online 17 April 2015

Keywords:
Local Green's function
Site-dependent load Love number
Surface deformation
Hydrological loading
Scatter plot

ABSTRACT

The influence of the elastic Earth properties on seasonal or shorter periodic surface deformations due to atmospheric surface pressure and terrestrial water storage variations is usually modeled by applying a local half-space model or an one dimensional spherical Earth model like PREM from which a unique set of elastic load Love numbers, or alternatively, elastic Green's functions are derived. The first model is valid only if load and observer almost coincide, the second model considers only the response of an average Earth structure. However, for surface loads with horizontal scales less than 2500 km^2, as for instance, for strong localized hydrological signals associated with heavy precipitation events and river floods, the Earth elastic response becomes very sensitive to inhomogeneities in the Earth crustal structure.

We derive a set of local Green's functions defined globally on a $1^\circ \times 1^\circ$ grid for the 3-layer crustal structure TEA12. Local Green's functions show standard deviations of ±12% in the vertical and ±21% in the horizontal directions for distances in the range from 0.1° to 0.5°. By means of Green's function scatter plots, we analyze the dependence of the load response to various crustal rocks and layer thicknesses. The application of local Green's functions instead of a mean global Green's function introduces a variability of 0.5–1.0 mm into the hydrological loading displacements, both in vertical and in horizontal directions. Maximum changes due to the local crustal structures are from −25% to +26% in the vertical and −91% to +55% in the horizontal displacements. In addition, the horizontal displacement can change its direction significantly. The lateral deviations in surface deformation due to local crustal elastic properties are found to be much larger than the differences between various commonly used one-dimensional Earth models.

1. Introduction

Temporal mass changes in the Earth system, that reflect changes in atmospheric surface pressure, ocean bottom pressure, and terrestrial water storage, lead to both gravity field variations and deformations at the Earth's surface, which are associated with the mass redistribution at the surface and the respective loading response of the Earth's interior. In contrast to tidal-induced surface mass variations, which are dominated by ocean processes, non-tidal mass variations with subdaily to seasonal periods are primarily acting over land as they are caused by atmospheric circulation and hydrological mass transport (e.g. Tregoning et al., 2009; Rajner and Liwosz, 2011; Fritsche et al., 2012). The global-scale gravity field variations are observed by the Gravity Recovery and Climate Experiment (GRACE) satellite mission, whereas space geodetic techniques such as the Global Positioning System (GPS), Very Long Baseline Interferometry (VLBI) and Satellite Laser Ranging allow the measurements of site position displacement. Atmospheric surface pressure and terrestrial water storage generate elastic deformations that are large enough to be detected with space geodetic techniques on global (Blewitt et al., 2001), regional (Fu et al., 2012) and local scales (Bevis, 2005). Elastic surface deformations have to be taken into account for the realization of terrestrial reference frames as they can affect epoch-wise parameters causing a significant loss in solution accuracy (Dach and Dietrich, 2000), or for the correction of regional geodetic surveys.

Site-specific load deformations can be calculated from observed or simulated atmospheric and hydrological mass variations. As mass variations induce deformation fields of principally global

* Corresponding author. Tel.: +49 331 288 1750.
E-mail address: dill@gfz-potsdam.de (R. Dill).

http://dx.doi.org/10.1016/j.jog.2015.04.005
0264-3707/

extent, a large area around each station has to be taken into account. Global mass re-distributions are accessible from global numerical weather models, global hydrospheric models, or can be derived from gravity field variations as given by the satellite mission GRACE (Van Dam et al., 2007, 2011). The displacement fields due to short-periodic surface loading processes are calculated with numerical models using the load Love numbers, or the Green's function approach introduced by Farrell (1972). Load Love numbers represent the spectral elastic response of a spherically symmetric, layered Earth structure to a unit mass that loads the Earth surface at the north pole. Widely used Earth's models are G–B (Gutenberg–Bullen A: see e.g. Alterman et al., 1961), PREM (Dziewonski and Anderson, 1981), or ak135 (Kennett, 1995). To derive Green's functions from the corresponding load Love numbers, the Earth's response to a point-load is calculated under the assumption that the elastic properties do not differ laterally. This implies that the considered loads extend over thousands of km. The sensitivity of the elastic response to inhomogeneities in the Earth's crust increases significantly for surface loads with horizontal scales less than 2500 km^2, such as hydrological mass load signals associated with heavy precipitation events, river floods, and the periodic filling of dams. Therefore, displacement signals observed by GPS (Jiang et al., 2013; Williams and Penna, 2011; Rajner and Liwosz, 2011) and VLBI (Petrov and Boy, 2004) reveal site-specific signatures originating from distinctive characteristics of the shallow elastic structure of the Earth's crust beneath the station (e.g. Fu et al., 2012; Bevis, 2005), an aspect which is not considered in traditional loading calculations based on Green's functions. According to their designated application, the traditional Green's functions are often only roughly categorized, e.g. into only soft, medium, or hard crustal rheologies (Wang et al., 2012). Although such models are rather common in geodetic applications, they suffer from their global 1-dimensional symmetry.

Wang (2000) constructed site-dependent Green's functions based on a local layered crustal structure consisting of sediments, crystalline basement, middle crust, and lower crust in order to provide load correction models for GPS observations in the front Three Gorges Reservoir area that are accurate enough to discriminate between earthquake-related crustal motion and height changes that occur due to reservoir impoundment (Wang et al., 2002). Gegout (2013) followed the same approach to present site-dependent Love numbers for specific geodetic observation sites taking into account the specific radial Earth structure below each site. Implicitly, this approach assumes spherically symmetric Earth models, each with the respective site-specific crustal structure. Recently, Wang et al. (2013) and Chanard et al. (2014) followed the reverse strategy and inferred an averaged elastic Earth structure for the Himalayan region from the consideration of observed loading processes.

In this study, we will resume the approach of site-dependent Green's functions, but not only for a small number of geodetic site locations but for a global assessment of uncertainties in calculating atmospheric and hydrological loading displacements.

Based on the laterally variable continental crust model provided by Tesauro et al. (2012) (here named TEA12), we determined local Green's functions on a global regular grid, see Section 2. The deviation of the local response from that of the 1-dimensional Earth models is discussed in Section 3 together with their applicability to the global representation of hydrological water loads including local structures like rivers and lakes as well as regional loads due to soil moisture or snow accumulation. In Section 4 a one-year simulation of global hydrological and non-tidal atmospheric loading is presented in order to figure out the maximum influences of crustal inhomogeneities on geodetic displacement observations.

2. Determination of local Green's functions

When discussing load responses induced by short-periodic mass variations like terrestrial water storage or atmospheric surface pressure variations with subdaily to annual periods, the purely elastic response of the Earth is a good first order approximation. Anelasticity or viscoelasticity, which have to be considered for processes like postseismic deformation or postglacial rebound, take place on longer time scales and will be neglected here. Assuming only purely elastic deformation, the response is instantaneous and superposition principle can be applied. Representing the surface-mass load in spherical harmonic coefficients of Legendre degrees, n, and order, m, its changes can be related to the spherical harmonic coefficients of the vertical and horizontal deformations, and geoid changes through degree-dependent load Love numbers. Farrell (1972) outlines the calculation of properly weighted sums of the load Love numbers for a given Earth model to form Green's functions. For a unit point mass, 1 kg, the vertical (radial) displacement, G_r, and horizontal displacement, G_h, at a distance Θ from the point mass can be derived from the load Love numbers h_n and l_n by

$$\begin{aligned} G_r(\Theta) &= \frac{a}{m_e}\sum_{n=0}^{\infty} h_n\, P_n(\cos\Theta) \\ G_h(\Theta) &= \frac{a}{m_e}\sum_{n=1}^{\infty} l_n\, \frac{\partial P_n(\cos\Theta)}{\partial\Theta} \end{aligned} \tag{1}$$

with Earth's radius a and Earth's mass m_e. Similarly, Green's functions for other quantities like the gravity change, strain, or tilt caused by a surface-mass load can be derived (not discussed in this study).

Assigning Eq. (1) to any extended mass distribution, the displacement field, $\boldsymbol{u}$, is given by a convolution integral over the loaded region, Ω, as

$$\begin{aligned} u_r(\boldsymbol{r}') &= \int_\Omega G_r(\Theta)\, L(\boldsymbol{r})\, d\Omega, \\ \boldsymbol{u}_h(\boldsymbol{r}') &= \int_\Omega \hat{q}(\boldsymbol{r},\boldsymbol{r}')\, G_h(\Theta)\, L(\boldsymbol{r})\, d\Omega. \end{aligned} \tag{2}$$

Here, $L(\boldsymbol{r})$ denotes the surface mass load at the location $\boldsymbol{r}(a, \lambda, \varphi)$ with longitude λ and latitude φ, $\boldsymbol{r} \in \Omega$. $\boldsymbol{r}'$ denotes an observation point (station), and $\hat{q}(\boldsymbol{r}, \boldsymbol{r}')$ is the unit vector originating from the station, tangential to the Earth's surface, which lies in the plane determined by the radius vectors to the station and to the mass load. The distance Θ between mass load and station is given by the angular distance $\Theta = \arccos(\boldsymbol{r} \cdot \boldsymbol{r}'/a^2)$.

As the convolution takes place in the spatial domain, the Green's function approach is especially useful if the spherical harmonic representation of the surface-mass load is dominated by high-degree Stokes Coefficients ($n > 1000$), as for instance, in the case of the highly heterogeneous distribution of terrestrial water storage.

In the calculation of load Love numbers, a customary idealization of the Earth is a model composed of spherically symmetric layers. The various acceptable global Earth models differ only slightly in their low-degree response. For higher degrees, the geological structure of the crust becomes relatively important. As consequence, a single spherically symmetric Earth model cannot represent the Earth's extremely heterogeneous outermost 50 km accurately enough for small-scale surface loads. For local geodetic deformation studies, one needs to re-compute the Green's functions from a set of load Love numbers valid for the specific region that considers the regional deviation of the Earth's elastic response with respect to the global mean. Introducing such locally defined

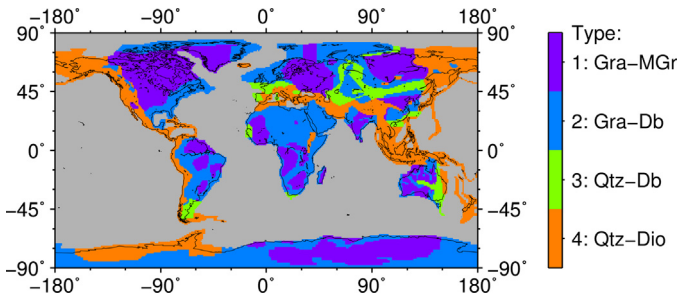

Fig. 1. Distribution of continental crust types in the model TEA12 (Tesauro et al., 2012). Color scale denotes the respective rock material for the two layers associated with the crystalline upper crust and lower crust (Gra – granite, MGr – mafic granulite, Db – diabase, Qtz – quartzite and Dio – diorite) overlaid by sediments of variable thickness. (For interpretation of the references to color in this figure legend, the reader is referred to the web version of the article.)

Green's functions $G(\Theta, \boldsymbol{r})$ (local Green's functions), the surface displacement at $\boldsymbol{r}'$ follows from the convolutions

$$u_r(\boldsymbol{r}') = \int_\Omega G_r(\Theta, \boldsymbol{r})\, L(\boldsymbol{r})\, d\Omega,$$
$$\boldsymbol{u}_h(\boldsymbol{r}') = \int_\Omega \hat{q}(\boldsymbol{r}, \boldsymbol{r}')\, G_h(\Theta, \boldsymbol{r})\, L(\boldsymbol{r})\, d\Omega. \quad (3)$$

In comparison to Eq. (2), the Green's functions now depend additionally on the location $\boldsymbol{r}(a, \lambda, \varphi)$ of the considered point-load for which the respective Earth structure beneath is assumed.

Local Green's functions are calculated from a Love number spectrum for each location applying a spherically symmetric Earth model that represents the specific elastic properties of the Earth crust in the respective region. The set up of these local Earth models is based on the PREM Earth model in which we replaced the uppermost 71 km by the lateral variability given in the crustal model TEA12 (Fig. 1) provided by Tesauro et al. (2012). TEA12 describes the Earth's crust (down to Moho depth) with one sedimentary layer and two layers of the crystalline crust on a uniform grid of $1^\circ \times 1^\circ$. The Moho depth is based on the global model CRUST 2.0 (Bassin et al., 2000), augmented in North America, Eurasia and Australia by newer high resolution compilations (Tesauro et al., 2008; Mooney and Kaban, 2010). Other parameters of the crust such as the global map of sediments for the continents (Tesauro et al., 2008; Mooney and Kaban, 2010) and oceans (NOOA, 2010 http://www.ngdc.noaa.gov/mgg/sedthick/sedthick.html) have also been revised with respect to CRUST2.0. Between the variable depth of the Moho estimated by TEA12 and the constant interface-depth with the 1-D PREM structure of 71 km, the upper mantle is assumed to have the lithology of a dry Olivine (Tesauro et al., 2012). As the TEA12 model was designed for the study of rheological structures of the crystalline crust, the authors divided the continental crust into four continental crust types and one oceanic crust type, where each layer of a specific type has a distinctive lithology. In order to evaluate the elastic behavior of the crust, the densities and seismic velocities for the lithology defined in TEA12 are taken from Christensen and Mooney (1995), see Table 1. For the sedimentary layer we associate the values of density and seismic velocities defined for the uppermost layer of PREM, without considering possible lateral variations. This choice seems simplistic in comparison to the recent CRUST1.0 model (Laske et al., 2012), where the crust is subdivided into six layers and their respective rocks and where especially the sediments differ strongly in their elastic parameters. However our approach has the advantage of a presentable amount of parameters. The deformational behavior depends only on the lithology of the two layers associated to the crystalline crust, their thicknesses, and the varying thickness of the sedimentary layer. The influence of the upper and lower crust is not masked by lateral heterogeneities of the sediments. For a quantitative analysis by means of a Green's functions scatter plot matrix, see Section 3.

Table 1
Elastic parameters of considered rocks chosen from Christensen and Mooney (1995). The sediments, not part of TEA12, are parametrized by PREM.

Rock	Density (kg/m^3)	V_p (km/s)	V_s (km/s)
Sediments (Sed)	2600	5.800	3.200
Granite (Gra)	2652	6.246	3.669
Quarzite (Qtz)	2652	5.963	4.035
Mafic granulite (MGr)	2971	6.839	3.767
Diabase (Db)	2936	6.712	3.729
Diorite (Dio)	2810	6.497	3.693
Olivine (Olv)	3438	8.455	4.523

Due to the fact that we will superimpose different Earth structures Section (4), we have to ensure that the total mass of each Earth structure keeps invariant and the radius of each Earth structure does not change. Therefore, the deviation in total mass along the Earth radius between PREM and the local density profile is corrected for by a slight adjustment of the core density. The core-mantle-boundary position is fixed. This approach tends to keep the low degree Love numbers that are determined by the Earth's whole structure whereas the higher-degree Love numbers, reflecting strongly the Earth's shallow structures, are not affected (Sung-Ho and Jeongho, 2011).

Each location on the Earth is represented by one member of these Earth models. For each Earth model a set of elastic gravitational differential equations relates density and seismic velocities to the deformational properties. This field equations can be solved for a self-gravitating elastic compressible and spherical Earth model by a Runge–Kutta integrator as outlined in detail by Martinec (1999) for both elastic and viscoelastic Love numbers. Each calculated Love number spectra gives the elastic response of one Earth model to a surface load. The Love numbers are evaluated for Legendre degrees from 2 to 50,000, whereas for degree 1, we keep the original values determined for the PREM structure which are defined in the center of mass of the solid Earth (CE) reference frame. The crustal properties cause differences in the Love number spectra, increasing with the zonal harmonic degree n, most pronounced in the higher degrees 200–2000. As we focus in this study on loading calculations in the spatial domain, we will give a more comprehensive analysis of the individual Earth models and their differences in deformational behavior after calculating the local Green's functions. Higher degree Love numbers will affect the near-field values of the Green's functions. The local Green's functions follow from solving for the appropriate sums in Eq. (1).

3. Variability of local Green's functions

The local Green's function represents the Earth's structure as if the local crustal characteristics extent over the whole globe. This view is acceptable if the local crustal structure only affects the near-field part of the Green's function. Wang et al. (2012) calculated the load Love numbers for different Earth models that deviate in the elastic parameters of the crust but also at the 220 km discontinuity. They pointed out that the load Love numbers are quite different for degrees higher than 200 and they suggested to replace the upper layer of PREM or ak135 by the crustal structure of CRUST2.0 when using Green's function for distances $\Theta < 1.0^\circ$. In contrast to the load Love numbers, the Green's functions allow us to validate directly the assumption that the local crustal structure influences only the local displacement. Figs. 2 and 3 show all local Green's functions over the $1^\circ \times 1^\circ$ global grid (thin green lines) in comparison to the global Green's functions for the Earth models G–B (dashed blue) used by Farrell (1972) and ak135 (dashed orange). In addition, the mean of all local Green's functions over land areas

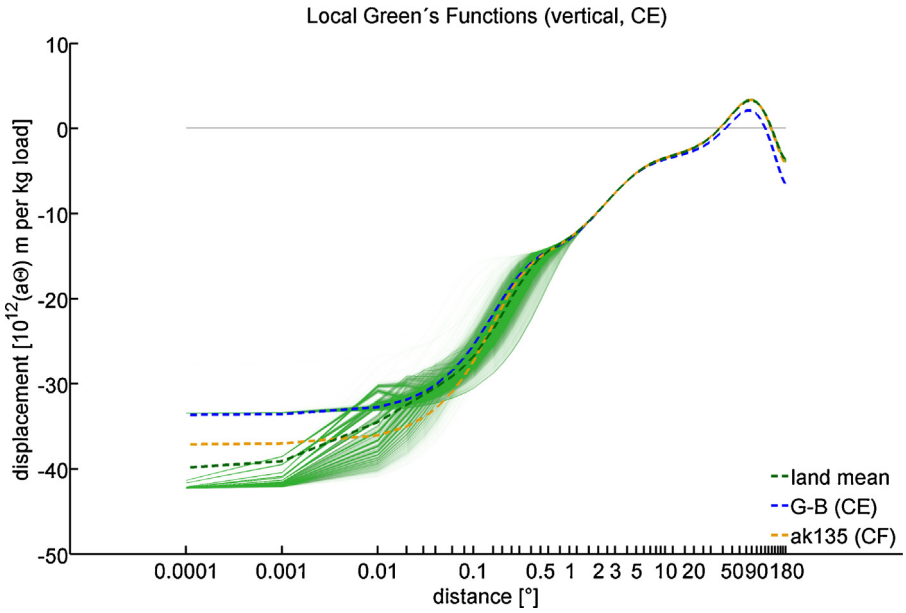

Fig. 2. Green's functions for vertical displacement. Green: Local Green's functions representing different crustal structures for every 1°×1°. Dashed green: Mean of all local Green's functions defined for continental crust. Dashed blue: Global Green's function for Earth model Gutenberg–Bullen A. Dashed orange: Global Green's function for Earth model ak135. (For interpretation of the references to color in this figure legend, the reader is referred to the web version of the article.)

(mean global Green's function) is given in dashed green and it is used in the remaining study as a reference to calculate the statistics such as the standard deviation. For distances $\Theta > 0.125°$, the mean global Green's function coincides well with ak135, but for smaller distances it does not coincide with any global model or crustal structure.

For the vertical displacement, the standard deviation of the local Green's functions from their mean global Green's function remains below 1% for distances $\Theta > 1.0°$. For the horizontal displacement, the standard deviation becomes lower than 1% only for $\Theta > 30°$ but it is within ±5% for $\Theta > 3.0°$. Hence, the near-field assumption is very well fulfilled for the vertical component $G_u(\Theta)$, but for $G_v(\Theta)$ the local crustal structure has still slight influences on the calculated displacements from $\Theta = 3°$ up to 30°. For distances $\Theta < 3°$, the local crustal structure becomes very important for the Green's functions amplitude. As expected, the lower crustal properties influence the Green's function for medium distances, whereas the uppermost properties, like sediment thickness influences only the very local Green's function (<0.1°).

A detailed view on the dependence of the Green's function on the internal crustal structure can be attained from scatter-plot matrices. Figs. 4 and 5 show the Green's function amplitudes in relation to the individual properties and thicknesses of the crustal layers sediments, upper crust, and lower crust. The scatter-plot matrices give a profile of the local Green's functions for the vertical and horizontal displacement at a distance of $\Theta = 0.25°$. This distance is chosen such that it is in the range between the standard resolution of global hydrological models of 0.5° and the highest resolution of the river mass distribution from the LSDM model of 0.125°. A compilation of scatter-plot matrices over the whole range of distances

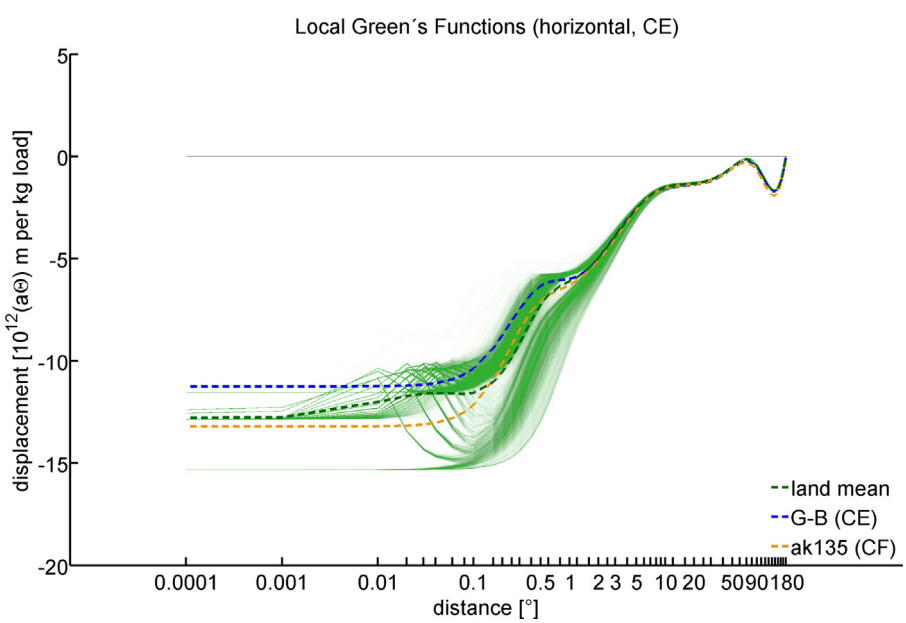

Fig. 3. Green's functions for horizontal displacement. For details see Fig. 2.

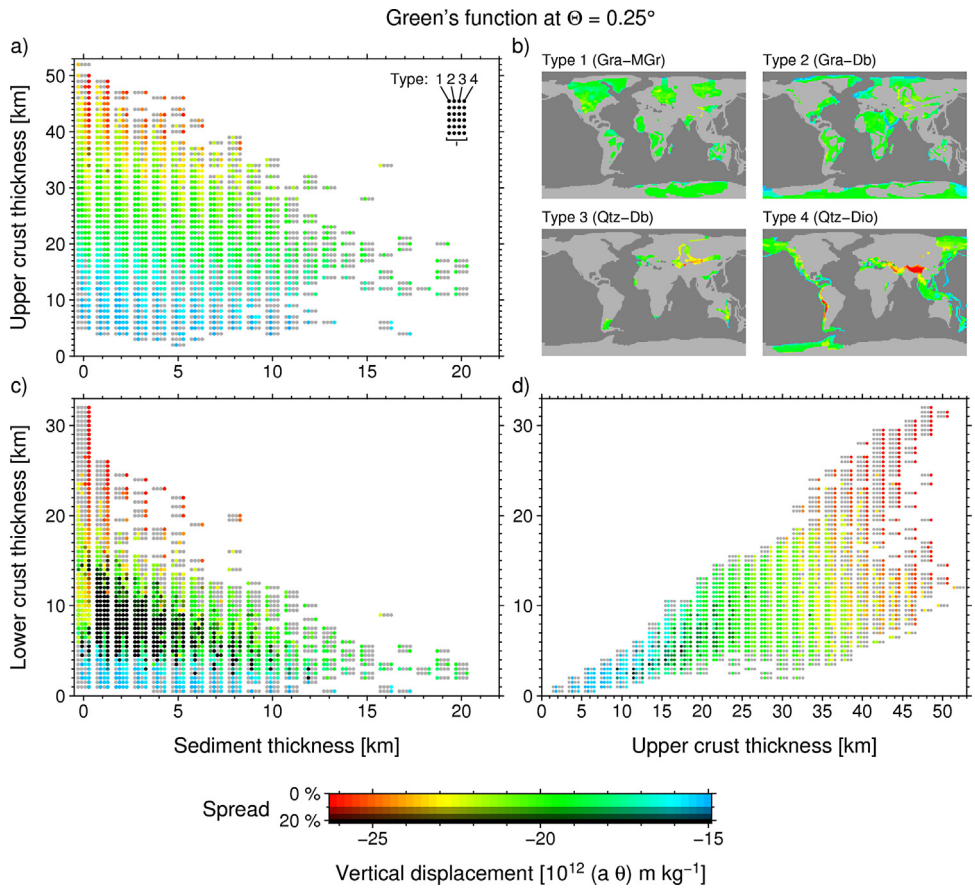

Fig. 4. Scatter-plot matrix of local Green's functions for vertical displacement at 0.25° distance for the 3-layer and 4-type crustal model TEA12. Each scatter plot (a), (c) and (d) shows the dependence on two layer thicknesses whereas the local Green's function values are averaged over the 3rd hidden dimension, respectively. The actual value is indicated in the unique color scale at the bottom. Full colors are darkened with increasing relative spread (max–min)/mean, due to the hidden dimension and turns into black if the relative spread exceeds 20%. Each crust type is represented separately in the quadruples. Quadruples are left out, if no type exists for a specific parameter combination, light grey shows missing values for respective parameter pairs and type. (b) Shows separately the geographical distribution for each type in the same color scale. (For interpretation of the references to color in this figure legend, the reader is referred to the web version of the article.)

from 0.0001° to 180° can be found in the supplement as movies. Each scatter plot illustrates the dependence of the Green's function amplitude on two out of three crustal layer thicknesses. The colors give the mean value, determined from all different Green's function values occurring due to variations in the 3rd hidden dimension, and its spread defined as the difference of the respective maximum and minimum values relative to the mean. As the shown value is only meaningful if the spread is small, the dot colors are darkened for an increasing spread. The color bar is unique for all plots specifying the respective range of displacements. In order to distinguish the crust types, the Green's functions in (a), (c) and (d) are split into the four types given in Fig. 1, diagrammed as columns of quadruples, one column for each thickness value along the abscissa. For better readability we applied a coarser resolution on the abscissa than in the original data, where the layer thicknesses are split into 0.5 km intervals. The geographic distribution is mapped in panel (b) for each crust type separately. From the scatter plots (a) and (c), we can investigate the influence of the sediment thickness. Variations of the Green's function amplitude within a row indicate a small influence even at $\Theta = 0.25°$; increasing sediment thickness leads to slightly enhanced displacements. For each crust type and given sediment thicknesses, the Green's function amplitudes increase for the vertical as for the horizontal displacement with the upper crust thickness, where types 3 and 4 show little more variation than types 1 and 2. These two groups of crustal types, see also similar colors in the maps of panel (b), differ only by their upper crust rock, granite or quartzite. Comparing panels a) and (c), the lower crust thickness has a comparable influence as the upper crust thickness. Panel (d) exposes that the upper and lower crust thicknesses are fairly well correlated representing their correlated dependence on the total crustal thickness. The black dots in panel (c) indicate a significant spread of more than 20% between local Green's functions of equal sediment and lower crust thickness due to variations in the upper crust thickness. For medium lower crust thicknesses there exist a wide range of upper crust thicknesses in the considered TEA12 and the Green's function value depends on all three layer thicknesses.

Green's functions for the horizontal displacement show even more distinctly the dependence on the local structure of the crustal layers. Fading from small distances up to $\Theta = 10°$, see scatter-plot movies in the supplement, we found that the sediment layer influences the horizontal displacement up to Θ = 0.2–0.5°, the upper crust properties are reflected up to 1–2° and lower crust properties are visible up to Θ = 5–10°. For greater distances, the far-field Green's functions are determined by the Earth's mantle and the local crustal structure becomes negligible. In conclusion, the dominant influence on local Green's functions comes from the upper crust properties, rock and thickness, whereas sediment thickness becomes important for very short distances smaller than $\Theta = 0.1°$. Sediment material is not discriminated in this study, For extremely small distances, $\Theta < 0.001°$, the horizontal displacement splits into three distinct values, 11.5, 12.8 and 15.3 (Fig. 3), which reflect the different elastic behavior of granite, sediments and quartzite, respectively, but already at 0.01° the deviations due to the stratified crust becomes evident.

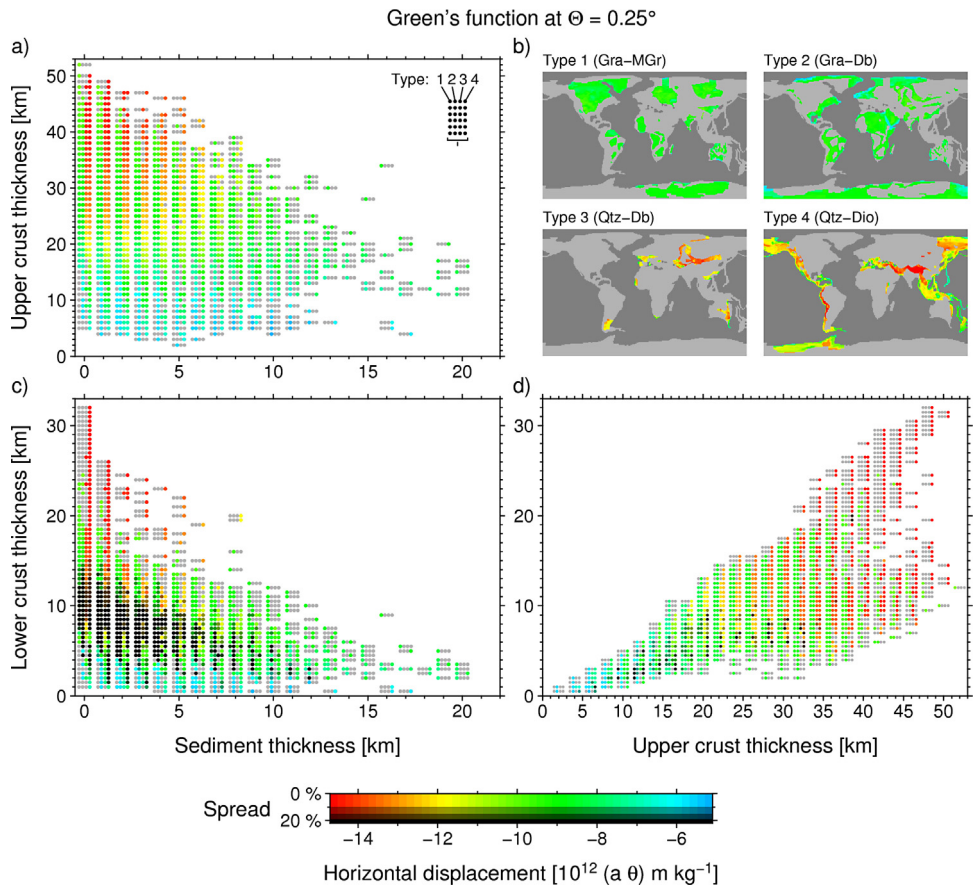

Fig. 5. Scatter-plot matrix of local Green's functions for horizontal displacement at 0.25° distance for the 3-layer and 4-type crustal model TEA12. For details see Fig. 4.

For hydrological loading applications, the variability of the local Green's functions in the range between Θ = 0.125–3° is the most important. For the vertical displacement at Θ = 0.25°, the differences from the mean value of −19.8 (ak135: −18.9) range from −32.1% to +24.5%. For the horizontal displacement, the differences from the mean value of −9.8 (ak135: −9.2) are even larger with −49% to 47%. The same range of differences is also present at Θ = 0.125°, from −14.3% to +40.9% and from −31.8% to +50.4% for vertical and horizontal displacements, respectively. Negative values indicate an enhanced displacement that can be

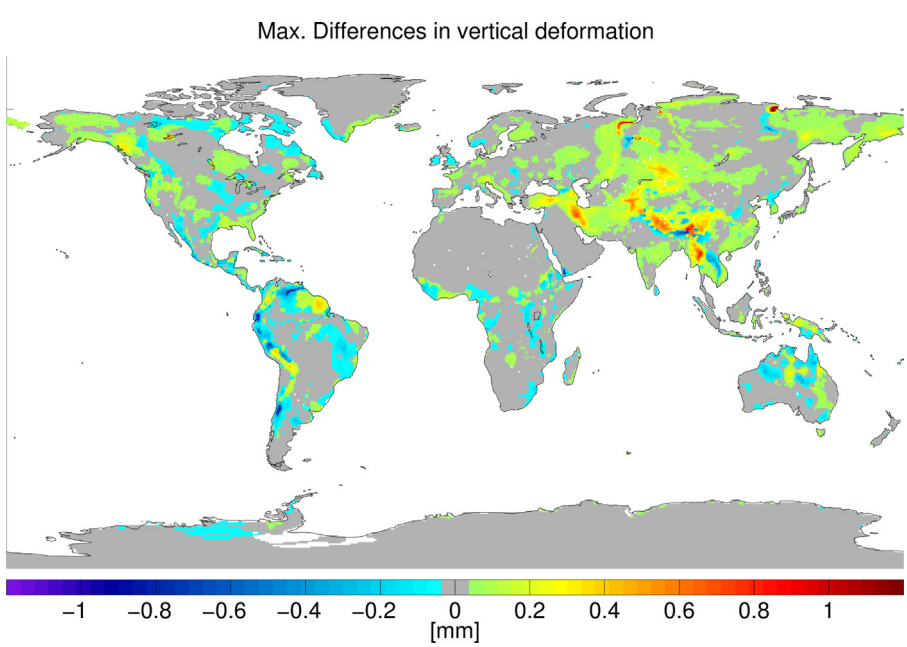

Fig. 6. Maximum differences in vertical hydrological loading displacements using local Green's functions and its continental mean over the year 2000.

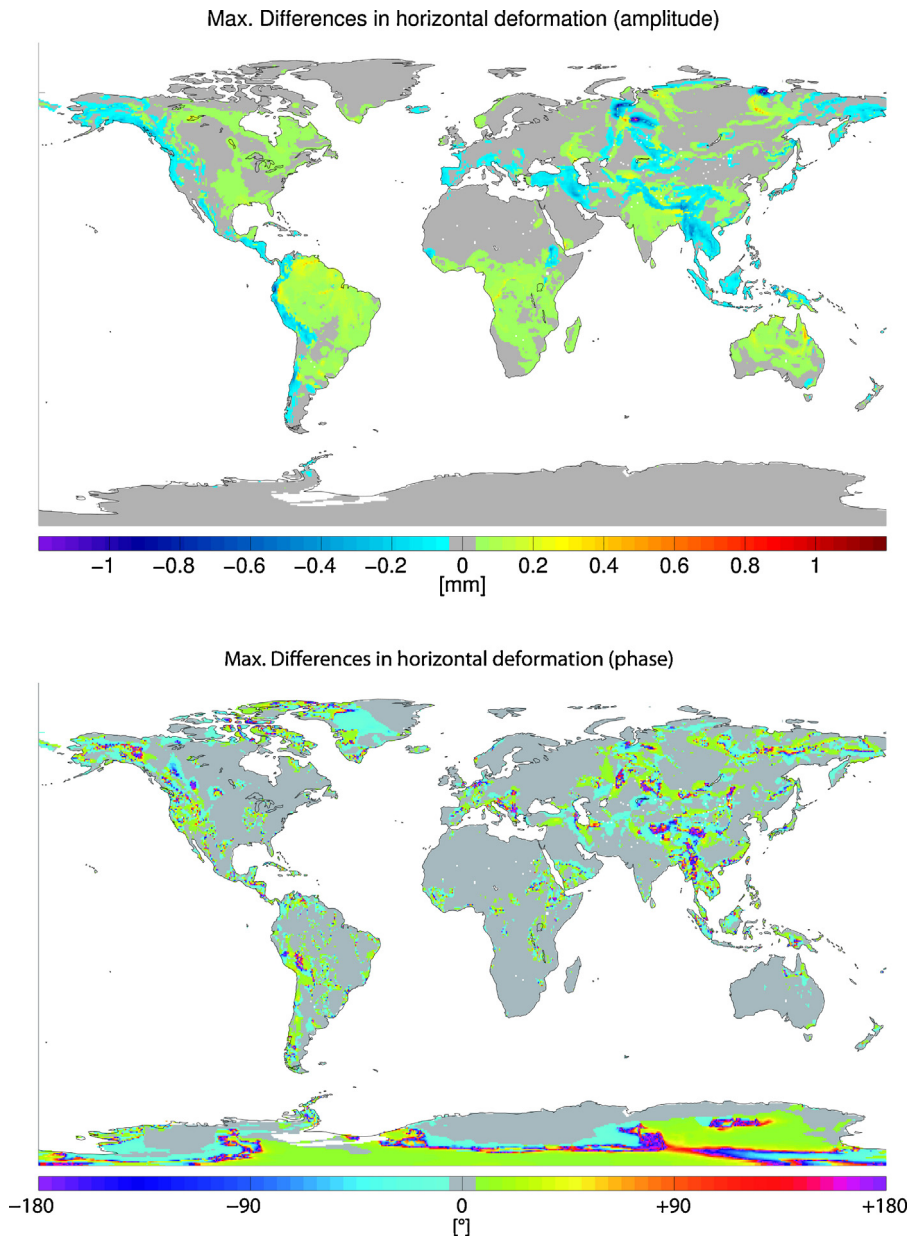

Fig. 7. Maximum differences in horizontal hydrological loading displacements (top: amplitude, bottom: phase) using local Green's functions and its continental mean over the year 2000.

found at locations with the thickest crust (≈80 km) of type 4, like the Himalayan and Andean orogene. Minimum displacements are located along the coast with crustal thicknesses smaller than 20 km.

4. Hydrological loading

In order to study the influence of local deviations of the crustal structure from a 1-dimensional model on load-induced surface deformations, we calculate the loading deformations due to one annual cycle of simulated terrestrial water storage variations. The global hydrological model LSDM (Land Surface Discharge Model: Dill, 2008) provides daily terrestrial water storage distributions of all hydrological compartments apart from deep groundwater on a 0.5°×0.5° global grid. To achieve a refined resolution of high inhomogeneous mass loads along the major river systems, the surface water masses from rivers and lakes are re-distributed from the 0.5° model grid to a finer resolution of 0.125° making use of HydroSHED river maps (Hydrological Data and Maps Based on Shuttle Elevation Derivatives at Multiple Scales; Lehner et al., 2008). Hydrological loading is then calculated for each day of the year 2000 for the 0.125°×0.125° LSDM terrestrial water storage variation using the patched Green's function approach (Dill and Dobslaw, 2013), where a high-resolution near-field convolution is combined with a low-resolution far-field convolution. The discussed local Green's functions, given on a 1.0°×1.0° global grid, are applied to the near-field, $\Theta < 3.5°$, according to Eq. (3). In the far-field we applied the mean global Green's function according to Eq. (2). For comparison, we carry out a reference calculation based solely on the mean global Green's function.

Loading results are given as daily time series for every 0.5°×0.5° gridpoint. The horizontal displacement vector, consisting of North-South and East-West components, is transformed into the amplitude and phase representations. For the following analysis, we form the differences between the new loading results using the local Green's functions and the reference solution.

Table 2
Differences between local Green's functions and mean global Greens function at $\Theta = 0.25^\circ$ and their influence on hydrological and non-tidal atmospheric loading.

	Vertical	Horizontal (Ampl.)
Green's function RMS	±2.9 (±12%)	±3.4 (±21%)
minimum	−6.3 (−32%)	−4.9 (−50%)
maximum	+5.0 (+24%)	+4.9 (+47%)
Hydrol. loading RMS	±0.5 mm (±17%)	±0.8 mm (±71%)
maximum	+1.5 mm (+26%)	+0.7 mm (+55%)
minimum	−1.2 mm (−25%)	−1.9 mm (−91%)
Atmosph. loading RMS	±0.2 mm (±05.1%)	±0.1 mm (±15.1%)
maximum	+0.56 mm (+23.8%)	+0.38 mm (+24.0%)
minimum	−0.54 mm (−08.6%)	−0.49 mm (−25.7%)

In Figs. 6 and 7 the maximum differences, signed positive or negative, that appear during one season are picked for each gridpoint. As expected, the greatest effects of the local Green's functions are at the locations where the highest water storage amplitudes occur together with greatest deviations of the local Green's function from the reference mean. In the Himalayan region, the differences in the vertical component of hydrological loading displacements reach +1.2 mm, mainly along the Brahmaputra river and the upper Yangzi river, indicating an increased loading effect due to thicker elastic crustal properties. At the Andean orogen, where no bigger river channels exist, the far-field loading effect of the Amazon basin with its slightly harder crustal properties leads to the decrease in loading amplitudes (−0.4 to −0.8 mm). Similarly, a slightly harder crust together with huge terrestrial water storage variations occur along the Orinoco river in northern South America, reaching additional −1.2 mm. The same situation can be found for example along the Amazon river and the lower Nile. On the other hand, most enhanced loading amplitudes are located at the Lena delta (+1.5 mm) and the lower Ob river where we find the crust types 3 and 4 (upper crust consisting of quartzite) together with a thick sediment layer and total crustal thicknesses around at least 50 km.

Although the Green's functions for the horizontal displacement are only half as large as for the vertical displacement, the differences in the horizontal displacement of hydrologically induced loading between the local Green's functions and the mean global Green's function are of the same order of magnitude as for the vertical displacement.

The highest horizontal loading amplitudes are located along the Lena and Ob rivers. Reduced amplitudes occur along the Amazon, the Congo, or the Volga rivers for example. As the horizontal displacement integrates all loading influences from all geographic directions and as the local Green's functions introduce a different weighting of the individual contributions, the phase (azimuth angle) is significantly affected by the regional crustal properties. There are many locations featuring the extreme case where the phase changes by $\pm 180^\circ$, meaning that the horizontal displacement turns to the opposite direction. Excluding locations where the horizontal displacement is very tiny, smaller than 1 mm, there remain still many location with phase changes of more than $\pm 175^\circ$, e.g. in Central Asia, along the Central Andes and the Rocky Mountains.

For the sake of completeness, we also calculate non-tidal atmospheric loading based on ECMWF atmospheric surface pressure data for the year 2000. As atmospheric surface loads extent over much larger areas than the hydrological loads, the atmospheric loading displacements depend more on regional-scale crustal structures, averaging local crustal properties over areas from 2.5° to 5°. In consequence, the influence of applying local Green's functions instead of a globally defined Green's function for atmospheric loading is not that noticeable like for hydrological loading, although the load amplitudes are of similar size, see Table 2.

5. Conclusion

In order to study the influence of local crustal elastic properties on site displacements due to surface-mass loads, hydrological loading was calculated for one year of modeled terrestrial water storage variations introducing locally defined Green's functions. These site-specific Green's functions are derived for a global 3-layer and 4-types crustal model (TEA12) which replaces the uppermost part of the Earth model PREM. Compared to more complex and detailed crustal models, like CRUST1.0, our setup allows a more systematic analysis of the influence of individual crustal layer properties such as rock material and thickness on the local Green's functions, and consequently on the hydrological loading displacements. For the analysis of the local Green's functions, we design the scatter-plot matrices, see Figs. 4 and 5 and movies in the supplement, which allow us to investigate the dependence on the crust type and thickness of individual layers. Local Green's functions show up significant deviations from a mean global Green's function for distances smaller than 1° and 3° for the vertical and horizontal displacements, respectively. Especially in the range of 0.125–0.5°, which is similar to the resolution of hydrological loads from global hydrological models, the Green's functions are very sensitive to the properties of the upper crust and to a lesser extent to the properties of the lower crust. In addition, the sediment layer cannot be neglected. In total, the Green's functions at distance $\Theta = 0.25^\circ$ vary by about 12% in the vertical and 21% in the horizontal components with maximum differences of 41% and 50%, respectively. Although the Green's functions for the horizontal displacement amount only to a half of the vertical component, the deviations in the modeled loading displacement due to local crustal elastic properties reach similar absolute values, around 1.0–1.5 mm for typical hydrological loads. Applying the local Green's functions instead of a mean global Green's function to non-tidal atmospheric surface pressure, the differences appear much smaller as the typical spatial wavelength of atmospheric mass load distributions is not that small as of hydrological loads and hence the local elastic properties of the sediment and the upper crust have less impact.

Our approach considers spatial variability in the Earth's crust material. The influence of anisotropy or lateral heterogeneity on the deformational behavior is not considered. The approximation seems to be valid as long as local crustal properties affect the elastic Earth response only in the near-field around the location of loading masses.

Introducing a site-dependent crustal response into surface displacement modeling provides a alternative way to probe the density and elastic structure of the Earth's crust and mantle by means of observed surface deformations. As different sediment thicknesses lead to completely different Green's functions in the near-field, typical deformation responses to local loads can be associated indirectly to the sediment layers beneath. Seitz and Krügel (2006) clustered local deformation patterns, derived from dense GPS observation networks (min. 20 station within a radius of 10°) into six significantly different loading responses of the Earth crust. Strong deformation signals with steep functions were supposed to arise from low densities in the shallow crust, slight deformations with flat functions were supposed to occur over high density structures. Based on our characterization of local Green's functions the different observed deformation responses could be related to individual properties in the Earth crustal layers. The other way around, realistic loading models can be used to determine mass variations of the hydrosphere and cryosphere from geodetically measured surface displacements, especially for mass variations in the spatial range between satellite resolution and in-situ observations that are rather difficult to monitor otherwise.

Acknowledgment

This work has been carried out within the framework of the research program 11/RFP.1/GEO/3309 financed by the Science Foundation of Ireland. ZM acknowledges this support.

Appendix A. Supplementary Data

Supplementary data associated with this article can be found, in the online version, at http://dx.doi.org/10.1016/j.jog.2015.04.005

References

Alterman, Z., Jarosch, H., Pekeris, C.L., 1961. Propagation of Rayleigh waves in the earth. Geophys. J. Int. 4 (1954), 219–241 http://gji.oxfordjournals.org/content/4/Supplement_1/219.short

Bassin, C., Laske, G., Masters, G., 2000. The current limits of resolution for surface wave tomography in North America. EOS Trans. AGU F897 81.

Bevis, M., 2005. Seasonal fluctuations in the mass of the Amazon River system and Earth's elastic response. Geophys. Res. Lett. 32 (16), 3–6 http://www.agu.org/pubs/crossref/2005/2005GL023491.shtml

Blewitt, G., Lavallée, D., Clarke, P., Nurutdinov, K., Dec. 2001. A new global mode of Earth deformation: seasonal cycle detected. Science (New York, NY) 294 (5550), 2342–2345 http://www.ncbi.nlm.nih.gov/pubmed/11743198

Chanard, K., Avouac, J.P., Ramillien, G., Genrich, J., 2014. Modeling deformation induced by seasonal variations of continental water in the Himalaya region: sensitivity to Earth elastic structure. J. Geophys. Res.: Solid Earth April http://doi.wiley.com/10.1002/2013JB010451

Christensen, N.I., Mooney, W.D., 1995. Seismic velocity structure and composition of the continental crust: a global view. J. Geophys. Res. 100 (B6), 9761 http://doi.wiley.com/10.1029/95JB00259

Dach, R., Dietrich, R., Sep. 2000. Influence of the ocean loading effect on GPS derived precipitable water vapor. Geophys. Res. Lett. 27 (18), 2953–2956, http://dx.doi.org/10.1029/1999GL010970 http://www.agu.org/pubs/crossref/2000../1999GL010970.shtml

Dill, R.,;1; 2008. Hydrological model LSDM for operational Earth rotation and gravity field variations. Str 08/09, GFZ, Potsdam. URL: http://www.google.de/url?sa=t&rct=j&q=hydrological model lsdm for operational earth rotation and gravity field variations&source=web&cd=1&ved=0CEcQFjAA&url=https://e-docs.geo-leo.de/bitstream/handle/11858/00-1735-0000-0001-3286-C/0809.pdf?sequence=1&ei=SbUrULm6GsndsgangoFo&usg=AFQjCNEkDvjtXYyBakG48b60-t2VFL5TOQ http://bib.gfz-potsdam.de/pub/str0809/0809.htm http://en.scientificcommons.org/37199196

Dill, R., Dobslaw, H., 2013. Numerical simulations of global-scale high-resolution hydrological crustal deformations. J. Geophys. Res.: Solid Earth 118 (August), 1–10, http://dx.doi.org/10.1002/jgrb.50353

Dziewonski, A.M., Anderson, D.L., Jun. 1981. Preliminary reference Earth model. Phys. Earth Planet. Inter. 25 (4), 297–356 http://linkinghub.elsevier.com/retrieve/pii/0031920181900467

Farrell, W.E., 1972. Deformation of the Earth by surface loads. Rev. Geophys. 10 (3), 761 http://www.agu.org/pubs/crossref/1972/RG010i003p00761.shtml

Fritsche, M., Döll, P., Dietrich, R., 2012, September. Global-scale validation of model-based load deformation of the Earth's crust from continental watermass and atmospheric pressure variations using GPS. J. Geodyn. 59–60, 133–142, http://dx.doi.org/10.1016/j.jog.2011.04.001

Fu, Y., Freymueller, J.T., Jensen, T., Mar. 2012. Seasonal and long-term vertical deformation in the Nepal Himalaya constrained by GPS and GRACE measurements. J. Geophys. Res. 117 (B3), L15310, http://dx.doi.org/10.1029/2011JB008925 http://www.agu.org/pubs/crossref/2012/2012GL052453.shtml

Fu, Y., Freymueller, J.T., Jensen, T., Aug. 2012. Seasonal hydrological loading in southern Alaska observed by GPS and GRACE. Geophys. Res. Lett. 39 (15), L15310, http://dx.doi.org/10.1029/2012GL052453 http://www.agu.org/pubs/crossref/2012/2012GL052453.shtml

Gegout, P., 2013. 2013. Earth's Elastic Deformation: Reference and Site-dependent Love Numbers. Tech. Rep. EGU General Assembly, EGU2013-4853.

Jiang, W., Li, Z., Dam, T., Ding, W., 2013. Comparative analysis of different environmental loading methods and their impacts on the GPS height time series. J. Geodesy 87 (May (7)), 687–703 http://link.springer.com/10.1007/s00190-013-0642-3

Kennett, B., 1995. Constraints on seismic velocities in the Earth from traveltimes. Geophys. J. Int., 108–124 http://gji.oxfordjournals.org/content/122/1/108.short

Laske, G., Masters, G., Ma, Z., Pasyanos, M.E., 2012. CRUST1.0: An Updated Global Model of Earth's Crust. Geophys Res Abstr 14, 3743 http://meetingorganizer.copernicus.org/EGU2012/EGU2012-3743-1.pdf

Lehner, B., Verdin, K., Jarvis, A., 2008. New global hydrography derived from spaceborne elevation data. EOS Trans. Am. Geophys. Union 89 (10) http://onlinelibrary.wiley.com/doi/10.1029/2008EO100001/abstract

Martinec, Z., 1999. Spectral, initial value approach for viscoelastic relaxation of a spherical earth with a three-dimensional viscosity – I. Theory. Geophys. J. Int. 137, 469–488.

Mooney, W.D., Kaban, M.K., 2010. The North American upper mantle: density, composition, and evolution. J. Geophys. Res. 115 (December (B12)), B12424, http://dx.doi.org/10.1029/2010JB000866

Petrov, L., Boy, J.-P., 2004. Study of the atmospheric pressure loading signal in very long baseline interferometry observations. J. Geophys. Res. 109 (B3), 1–14 http://arxiv.org/abs/physics/0311096, http://www.agu.org/pubs/crossref/2004/2003JB002500.shtmlhttp://www.agu.org/pubs/crossref/2004/2003JB002500.shtml

Rajner, M., Liwosz, T., 2011. Studies of crustal deformation due to hydrological loading on GPS height estimates. Geodesy Cartogr. 60 (January (2)), 135–144 http://versita.metapress.com/content/t21534116346m623/?referencesMode=Show, http://versita.metapress.com/openurl.asp?genre=article&id=doi:10.2478/v10277-012-0012-yhttp://versita.metapress.com/openurl.asp?genre=article&id=doi:10.2478/v10277-012-0012-y

Seitz, F., Krügel, M., 2006. Geodetic Reference Frames. International Association of Geodesy Symposia 134. Springer Verlag Berlin Heidelberg 2009. Ch. Inverse Model Approach for Vertical Load Deformations in Consideration of Crustal Inhomogeneities.

Sung-Ho, N., Jeongho, B., 2011. Computation of the Load Love Number and the Load Green's Function for an Elastic and Spherically Symmetric Earth. J. Korean Phys. Soc. 58 (May (5)), 1195 http://www.kps.or.kr/jkps/abstract_view.asp?articleuid=E01DF703-0D5A-437E-A543-185980F790C7

Tesauro, M., Audet, P., Kaban, M.K., Bürgmann, R., Cloetingh, S., 2012. The effective elastic thickness of the continental lithosphere: comparison between rheological and inverse approaches. Geochem. Geophys. Geosyst. 13 (September (9)), http://dx.doi.org/10.1029/2012GC004162

Tesauro, M., Kaban, M.K., Cloetingh, S.a.P.L., Mar. 2008. EuCRUST-07: a new reference model for the European crust. Geophys. Res. Lett. 35 (5), L05313, http://dx.doi.org/10.1029/2007GL032244

Tregoning, P., Watson, C., Ramillien, G., McQueen, H., Zhang, J., Aug. 2009. Detecting hydrologic deformation using GRACE and GPS. Geophys. Res. Lett. 36 (15), L15401 http://www.agu.org/pubs/crossref/2009/2009GL038718.shtml

Van Dam, T., Collieux, X., Altamimi, Z., Ray, J., 2011. A Review of GPS and GRACE Estimates of Surface Mass Loading Effects.

Van Dam, T., Wahr, J., Lavallée, D., 2007. A comparison of annual vertical crustal displacements from GPS and Gravity Recovery and Climate Experiment (GRACE) over Europe. J. Geophys. Res. 112 (B3), 1–11 http://www.agu.org/pubs/crossref/2007/2006JB004335.shtml

Wang, H., 2000. Surface vertical displacements and level plane changes in the front reservoir area caused by filling the three gorges reservoir. J. Geophys. Res.: Solid Earth 105 (B6), 13211–13220, http://dx.doi.org/10.1029/2000JB900072

Wang, H., Hsu, H.T., Zhu, Y.Z., 2002. Prediction of surface horizontal displacements, and gravity and tilt changes caused by filling the three gorges reservoir. J. Geodesy 76 (2), 105–114, http://dx.doi.org/10.1007/s00190-001-0228-3

Wang, H., Xiang, L., Jia, L., Jiang, L., Wang, Z., Hu, B., Gao, P., 2012, December. Load Love numbers and Green's functions for elastic Earth models PREM, iasp91, ak135, and modified models with refined crustal structure from Crust 2.0. Comput. Geosci. 49, 190–199 http://linkinghub.elsevier.com/retrieve/pii/S0098300412002245

Wang, H., Xiang, L., Wu, P., Steffen, H., Jia, L., Jiang, L., Shen, Q., 2013. Effects of the Tibetan plateau crustal structure on the inversion of water trend rates using simulated GRACE/GPS data. Terr. Atmos. Ocean. Sci. 24 (4-1), 505 http://tao.cgu.org.tw/index.php?doi=tao.2012.09.21.01.TibXS

Williams, S.D.P., Penna, N.T., 2011. Non-tidal ocean loading effects on geodetic GPS heights. Geophys. Res. Lett. 38 (May (9)), L09314 http://www.agu.org/pubs/crossref/2011/2011GL046940.shtml